Supporting Information for

A Redox-Active Luminescent Ytterbium Based Single Molecule Magnet

Fabrice Pointillart,* Boris Le Guennic, Stéphane Golhen, Olivier Cador, Olivier Maury and Lahcène Ouahab

EXPERIMENTAL PROCEDURES

General procedures and materials. All solvents were dried using standard procedures. $Yb(tta)_3.2H_2O$.[1] All other reagents were purchased from Aldrich Co. Ltd and were used without further purification.

Synthetic Procedure.

Procedure for synthesis of the ligand 4,5-Bis(thiomethyl)-4'-carboxylictetrathiafulvalene ($\mathbf{L^1}$)

$\mathbf{L^1}$ is obtained by de-esterification and alkaline hydrolysis from the 4,5-Bis(thiomethyl)-4',5'-bis(methoxycarbonyl)tetrathiafulvalene derivative.[2,3]

Procedure for synthesis of the ligand 4,5-Bis(thiomethyl)-4'-ortho-pyridyl-*N*-oxide-carbamoytetrathiafulvalene ($\mathbf{L^2}$)

4,5-Bis(thiomethyl)-4'-chlorocarbonyletrathiafulvalene[3] (120 mg, 0.28 mmol) is dissolved in 10 mL of distilled THF and then slowly added to a solution of 20 mL of distilled THF containing 2-aminopyridine-*N*-oxide[4] (61 mg, 0.56 mmol). The mixture was stirred during 4 hours at room temperature then the solvent was removed under vacuum. The excess of amine was removed from the solid residue by washing with water (3*20 mL). $\mathbf{L^2}$ was air dried and used without further purification. Yield: 53 mg (44 %).

Procedure for the reaction of coordination $[Yb(tta)_2(\mathbf{L^1})(\mathbf{L^2})]_2 \cdot 1.4(CH_2Cl_2)$

87.3 mg of $Yb(tta)_3 \cdot 2H_2O$ (0.1 mmol) were dissolved in 10 ml of CH_2Cl_2 and added to a 10 mL solution of CH_2Cl_2 containing a mixture (1:1 in molar ratio) of $\mathbf{L^1}$ (34.0 mg, 0.1 mmol) and $\mathbf{L^2}$ (43.2 mg, 0.1 mmol). After 45 minutes of stirring, the mixture was filtered, the filtrate was put in a closed flask and *n*-hexane was layered. After 5 days, pale orange single crystals were collected. Yield: 18 mg (24 %). Single crystals were suitable for X-ray diffraction study.

Crystal Structure Determination. Single crystal of $[Yb(tta)_2(\mathbf{L^1})(\mathbf{L^2})]_2 \cdot 1.4(CH_2Cl_2)$ was mounted on a APEXII Bruker-AXS diffractometer for data collection (MoKα radiation source, λ = 0.71073 Å), from the Centre de Diffractométrie (CDIFX), Université de Rennes 1, France. Structures were solved with a direct method using the SIR-97 program and refined with a full matrix least-squares method on F^2 using the SHELXL-97 program.[5] Crystallographic data are summarized in Table 1. CCDC 865604 contains the supplementary

crystallographic data for this paper. These data can be obtained free of charge from The Cambridge Crystallographic Data Centre via www.ccdc.cam.ac.uk/data_request/cif.
The 4,5-bis(methylthio)-1,3-dithiole part of ligand $\mathbf{L^1}$ is disorder into two positions labelled C19 to C22 and S9 to S12 for first one and C19M to C22M and S9M to S12M for the opposite. The occupation factor were calculated by employing site occupation factors of 21 and -21 respectively yielding to sof close to 0.7 and 0.3.
The dichloromethane solvatation molecule was first refined using 31 free variable, which yielded a value so close to 0.7. This indicate the impossibility for 4,5-bis(methylthio)-1,3-dithiole labelled "M" to be too close to dichloromethane solvent.

Electrochemical Measurements. Cyclic voltametry was carried out in CH_2Cl_2 solution, containing 0.1 M $N(C_4H_9)_4PF_6$ as supporting electrolyte. Voltamograms were recorded at 100 $mV.s^{-1}$ at a platinum wire electrode. The potentials were measured versus a saturated calomel electrode (SCE).

Solid State Absorption Measurements. Optical spectra were measured using the KBr disk method on Perkin-Elmer 1600 Series FT-IR (resolution 4 cm^{-1}) for infrared (IR). Absorption spectra were recorded on a Varian Cary 5000 UV-Visible-NIR spectrometer.

Solid State Luminescence Measurements. The luminescence spectra were measured using a Horiba-JobinYvon Fluorolog-3® spectrofluorimeter, equipped with a three slit double grating excitation and emission monochromator with dispersions of 2.1 nm/mm (1200 grooves/mm). The steady-state luminescence was excited by unpolarized light from a 450 W xenon CW lamp and detected at an angle of 90° for diluted solution measurements or at 22.5° for solid state measurement (front face detection) by a Peltier-cooled red-sensitive Hamamatsu R2658P photomultiplier tube (300-1010 nm). Spectra were reference corrected for both the excitation source light intensity variation (lamp and grating) and the emission spectral response (detector and grating). Uncorrected near infra-red spectra were recorded at an angle of 45° using a liquid nitrogen cooled, solid indium/gallium/arsenic detector (850-1600 nm) protected by a RG850 filter.

Magnetic dc and ac Measurements. The dc and ac magnetic susceptibility measurements were performed with a Quantum Design MPMS-XL SQUID magnetometer. The samples preparations consist of crashed selected single crystals dispersed in an eicosane matrix. For $\chi_M T$ vs. T the applied magnetic field is equal to 0.2 kOe between 2 and 20 K and 10 kOe above. The experimental data have been corrected from the diamagnetism of the sample holder (eicosan included), and the intrinsic diamagnetism of the materials was evaluated with Pascal's tables.

Computational Details. DFT geometry optimizations and TD-DFT excitation energy calculations of the ligands $\mathbf{L^1}$ and $\mathbf{L^2}$, and Y(III) dinuclear complex were carried out with the Gaussian 09 (revision A.02) package[6] employing the PBE0 hybrid functional.[7] The "Stuttgart/Dresden" basis sets and effective core potentials were used to describe the yttrium atom,[8] whereas all other atoms were described with the SVP basis sets.[9] The first 50 and 140 monoelectronic excitations were respectively calculated for the ligands $\mathbf{L^1}$, $\mathbf{L^2}$ and complex **2**. In all steps, a modeling of bulk solvent effects (solvent = dichloromethane) was included through the Polarisable Continuum Model (PCM),[10] using a linear-response non-equilibrium approach for the TD-DFT step.[11] Molecular orbitals were sketched using the Gabedit graphical interface.[12]

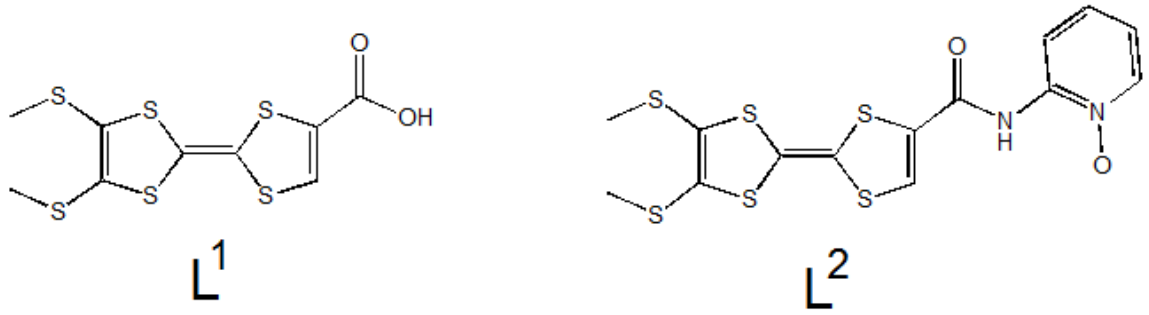

Fig. S1 Molecular representation of the ligands $\mathbf{L^1}$ and $\mathbf{L^2}$.

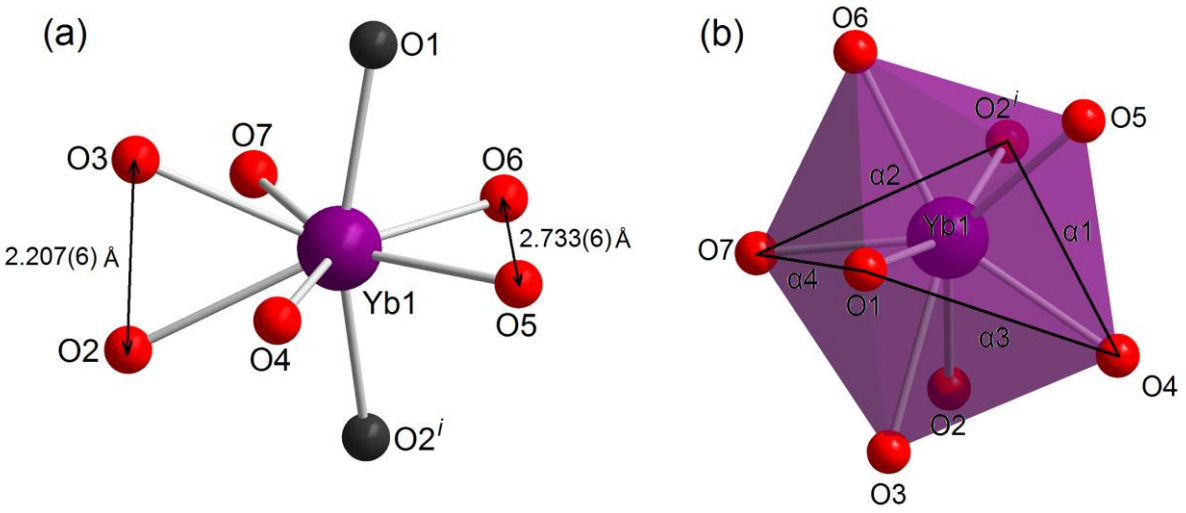

Fig. S2 (a) Central Yb(III) ions with its first neighbouring oxygen atoms. In red, are represented the "equatorial oxygen atoms" and in black are represented the "axial oxygen atoms". (b) Yb(III) polyhedron with characteristic α1- α4 angles associated with black lines. Symmetry used (i) 1–x, 1-y, -z.

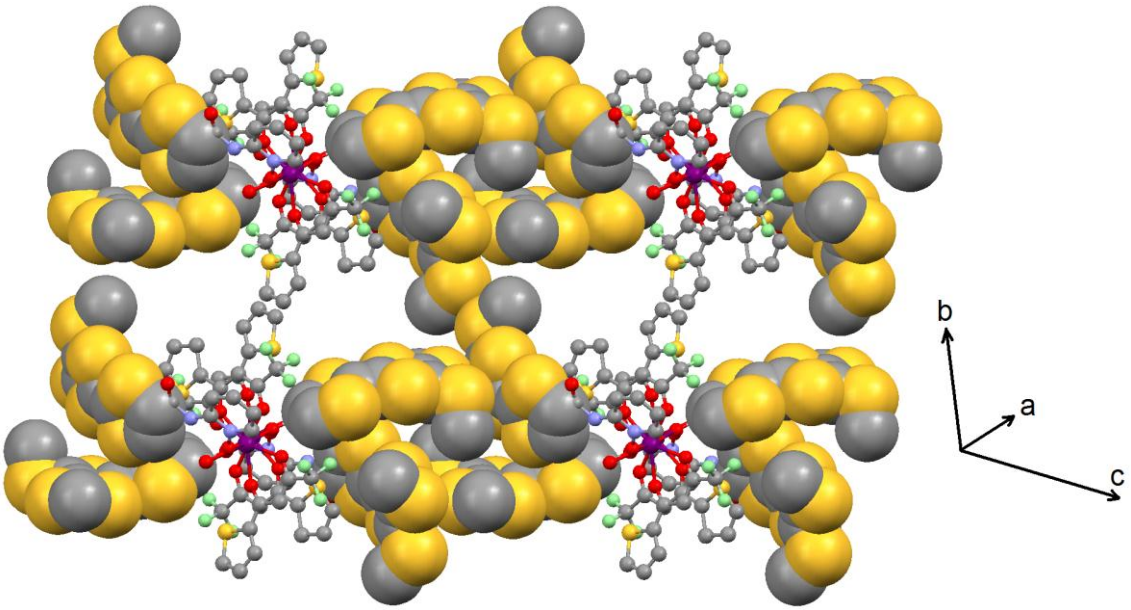

Fig. S3 Crystal packing highlighting the van der Waals contacts between the ligands $\mathbf{L^1}$ and $\mathbf{L^2}$.

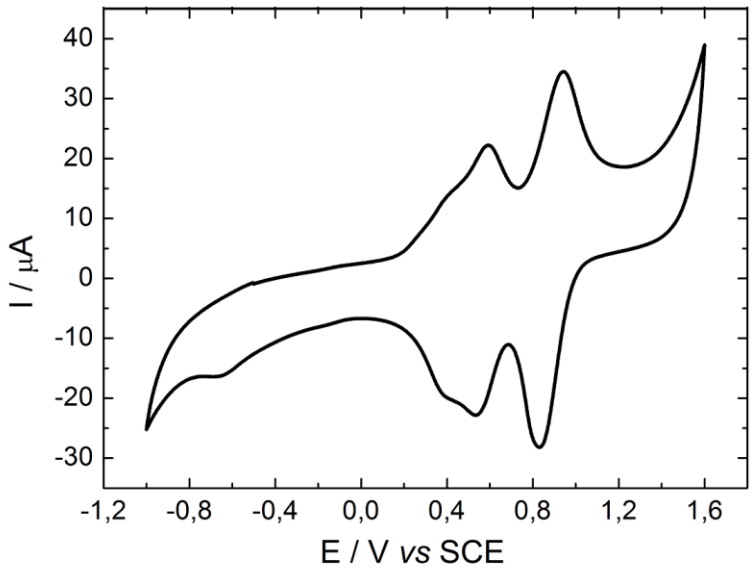

Fig. S4 Cyclic voltammetry of the compound $[Yb(tta)_2(\mathbf{L^1})(\mathbf{L^2})]_2 \cdot 1.4(CH_2Cl_2)$ in CH_2Cl_2 at a scan rate of 100 $mV.s^{-1}$.The potentials were measured *versus* a saturated calomel electrode (SCE); glassy carbon as the working electrode; Pt wire as the counter electrodes. It shows two mono-electronic oxidations at about 0.42 V and 0.57 V vs. SCE corresponding to the formation of TTF fragment radical cations for $\mathbf{L^1}$ and $\mathbf{L^2}$, respectively and one two-electronic oxidation at about 0.89 V corresponding to the formation of dicationic species simultaneously for $\mathbf{L^1}$ and $\mathbf{L^2}$.

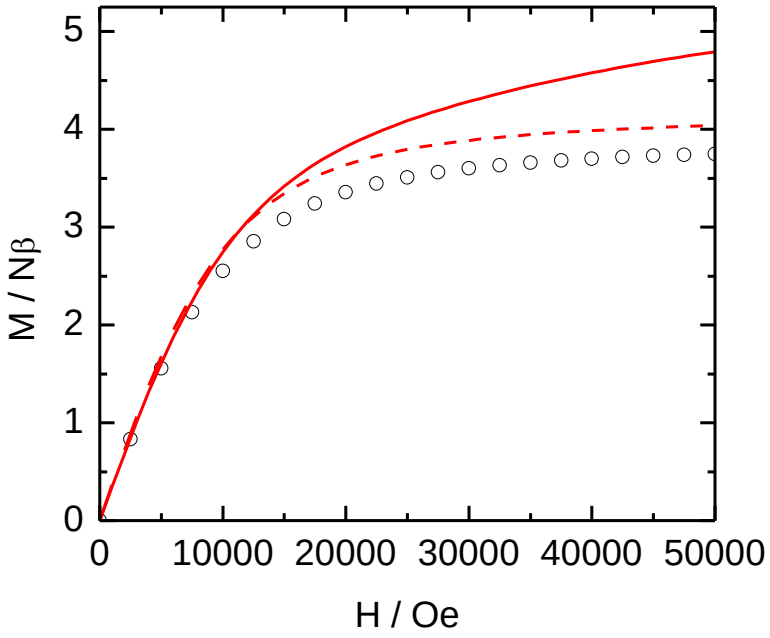

Fig. S5 Magnetic field dependence of the magnetization measured at T = 2 K (circles) with the calculated curve (full red lines) with the set of parameters given in main text. The dashed red line corresponds to the magnetization calculated with the $M_J = \pm 7/2$ states only (Ising).

Extended Debye model:

$$\chi' = \chi_S + (\chi_T - \chi_S)\frac{1+(\omega\tau)^{1-\alpha}\sin\left(\alpha\frac{\pi}{2}\right)}{1+2(\omega\tau)^{1-\alpha}\sin\left(\alpha\frac{\pi}{2}\right)+(\omega\tau)^{2-2\alpha}}$$

$$\chi'' = (\chi_T - \chi_S)\frac{(\omega\tau)^{1-\alpha}\cos\left(\alpha\frac{\pi}{2}\right)}{1+2(\omega\tau)^{1-\alpha}\sin\left(\alpha\frac{\pi}{2}\right)+(\omega\tau)^{2-2\alpha}}$$

With χ_T the isothermal susceptibility, χ_S the adiabatic susceptibility, τ the relaxation time, α an empirical parameters to account the distribution of the relaxation time and $\omega = 2\pi\nu$ with ν the frequency of the oscillating field. The best fitted parameters τ, α, χ_T, χ_S are listed in Table S1 with the coefficient of determination R^2. One example, at T = 2 K in zero applied field and within 2000 Oe, is given below:

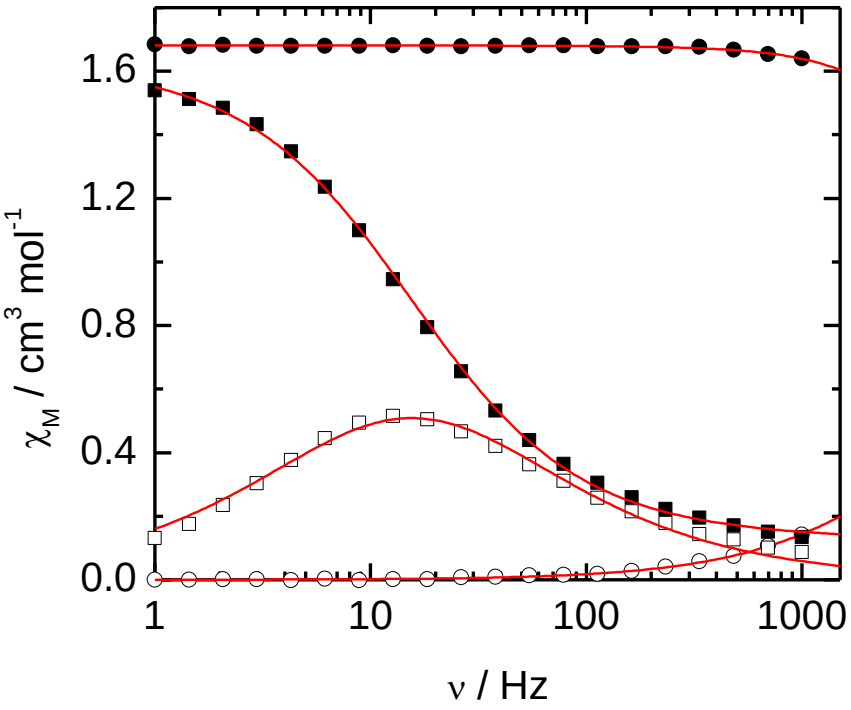

Fig. S6 Frequency dependence of the in-phase (full symbols) and out-of-phase (empty symbols) components of the ac susceptibility measured at 2 K in zero field (circles) and at 2000 Oe (squares) with the fitted curves (red lines) with the extended Debye model : χ_T = 1.6811(5) $cm^3\ mol^{-1}$, χ_S = 0.9(1) $cm^3\ mol^{-1}$, $\tau = 2.9(5)\times10^{-5}$ s and α = 0.06(1) in zero-field and χ_T = 1.64(1) $cm^3\ mol^{-1}$, χ_S = 0.124(7) $cm^3\ mol^{-1}$, τ = 0.0103(3) s and α = 0.24(1) at 2000 Oe.

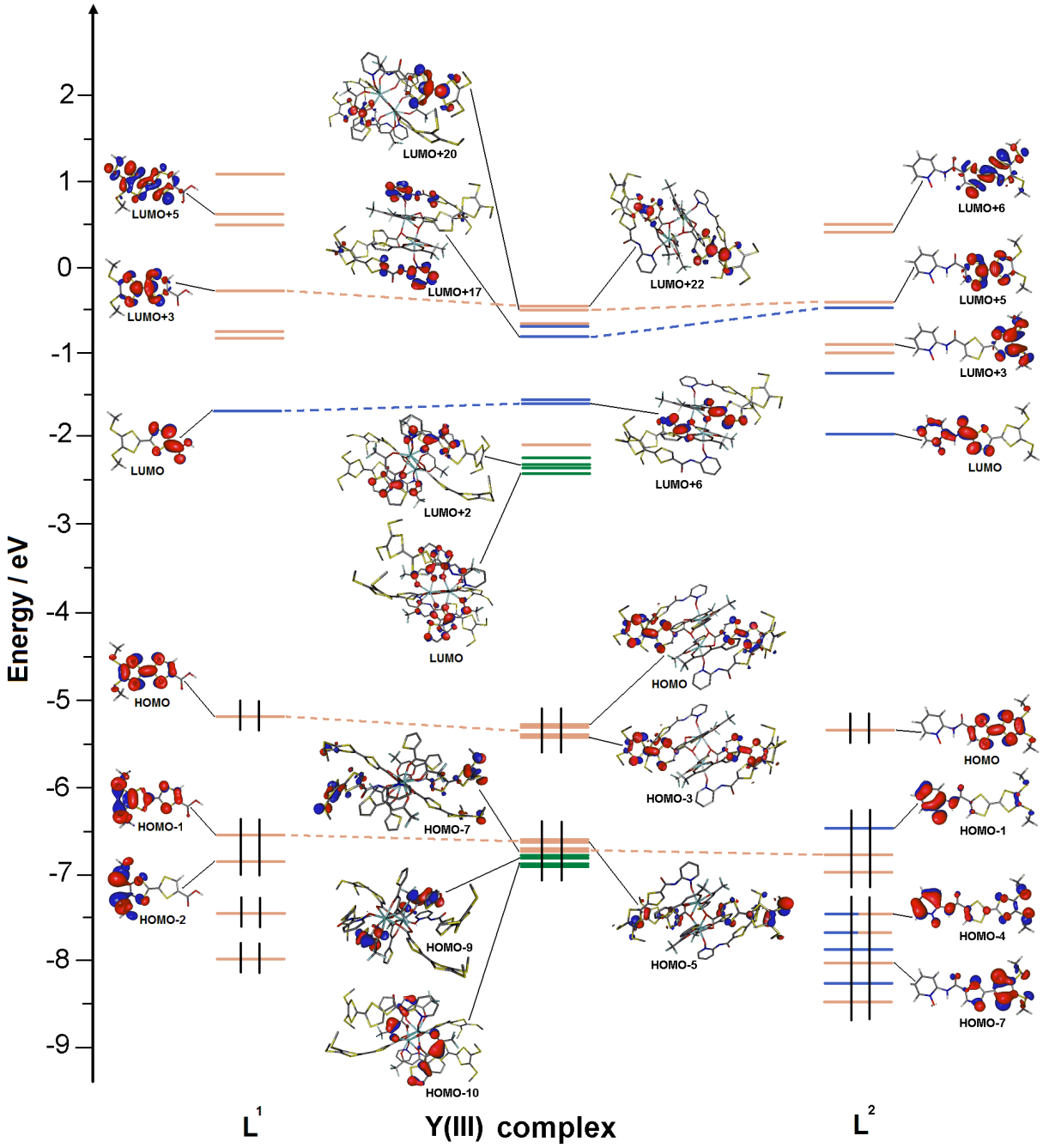

Fig. S7 MO diagram of L^1, L^2 and Y(III) analogue. Energy levels of the centered TTF, COO or amido-2-Py-*N*-oxide acceptors and tta^- orbitals are respectively represented in orange, blue and green color. Only selected molecular orbitals are drawn for the Y(III) complex.

Absorption properties of free ligands L^1 and L^2: The experimental absorption curve of L^1 was deconvoluted in six bands (Fig. 2a). The calculated UV-visible absorption spectrum for L^1 well reproduces the experimental curve except for the lowest-energy band which may be attributed to intermolecular charge transfers (Fig. 2a and 2d).[13] The low energy band was calculated at the average value of 22774 cm^{-1} (experimental value found at 22200 cm^{-1}, red Gaussian deconvolution) and attributed to π-π* HOMO → LUMO (98%) TTF to COOH charge transfers (ILCT) (Fig. S4, Table S2). The following four absorption bands centred at 27000 cm^{-1}, 33400 cm^{-1}, 39500 cm^{-1} and 45900 cm^{-1} (orange Gaussian deconvolutions) were calculated at the respective average energies of 33948 cm^{-1}, 35935 cm^{-1}, 39268 cm^{-1} and 45027 cm^{-1}. They are all attributed to π-π* and π-σ* intra-BTM-TTF transitions (ID) (Table S2). The experimental absorption curve of L^2 was deconvoluted in seven bands (Fig. 2b). Once again, the calculated UV-visible absorption spectrum for L^2 well reproduces the experimental curve except for the lowest-energy band which may also be attributed to intermolecular charge transfers (Fig. 2b and 2d).[13] The low energy band was calculated at the average value of 21233 cm^{-1} (experimental value found at 21500 cm^{-1}, red deconvolution) and attributed to π-π* HOMO → LUMO (98%) BTM-TTF to 2-Py-*N*-oxide charge transfers (ILCT) (Fig. S4, Table S2). The energy value of the ILCT in L^2 is lower than for L^1 because the pyridine-*N*-oxide is a better acceptor than the carboxylic moiety. The absorption band centred at 27900 cm^{-1} (blue deconvolution) was calculated at the average value of 30474 cm^{-1} and attributed to the π-π* HOMO-1 → LUMO (85%) intra-Py-*N*-oxide transitions (Table S2). The two next absorption bands centred at 32300 cm^{-1} and 35700 cm^{-1} (orange deconvolutions) were identified as intra-BTM-TTF (ID) transitions (Table S2). The blue Gaussian deconvolution centred at 38900 cm^{-1} was calculated at the average energy of 40197 cm^{-1} and meanly attributed to π-π* intra-Py-*N*-oxide (IA) transitions (Table S2). Finally the highest-energy large absorption band at 45700 cm^{-1} (red deconvolution) corresponds to the two excitations calculated at 43760 cm^{-1} and 46281 cm^{-1}, i.e., the π-π* BTM-TTF to Py-*N*-oxide ILCT (Table S2).

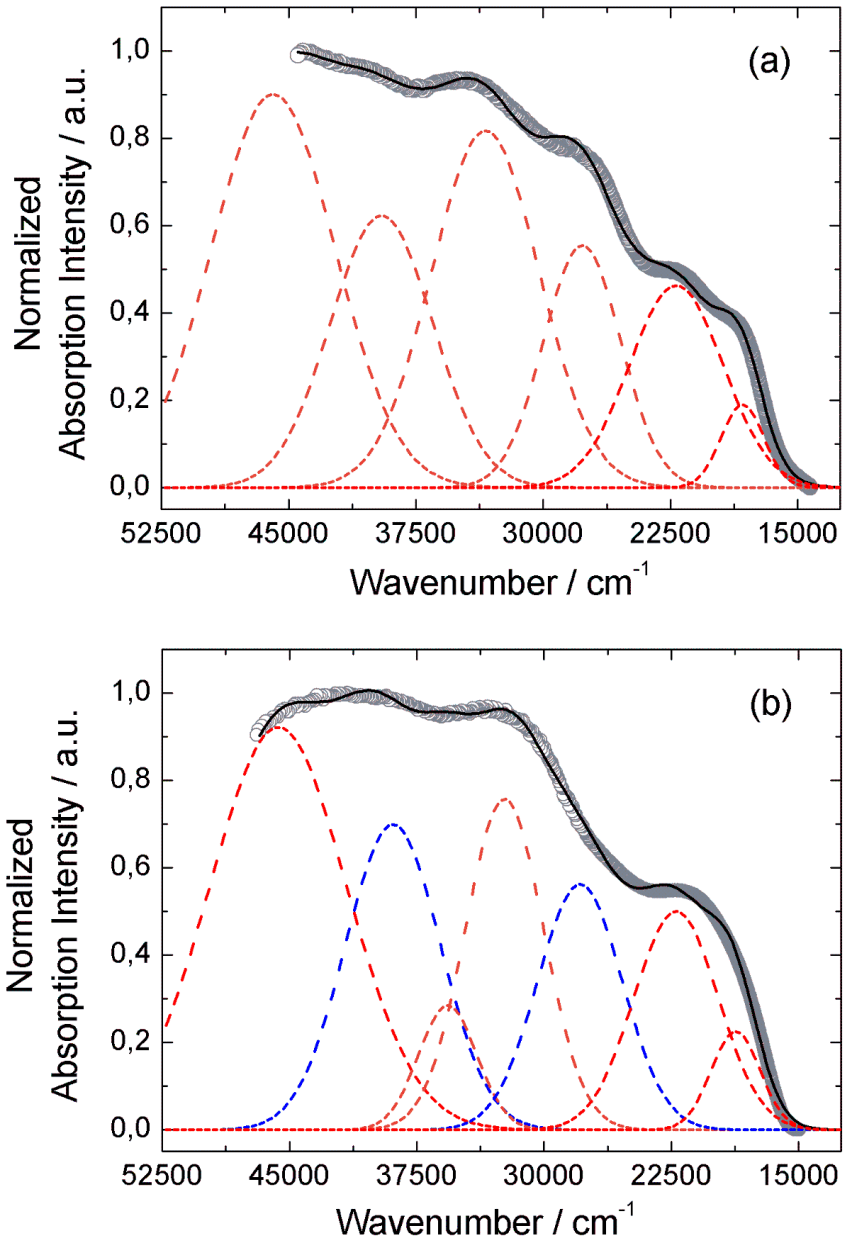

Fig. S8. Experimental UV-visible absorption spectra in solid-state (KBr pellets) of compounds $\mathbf{L^1}$ (a) and $\mathbf{L^2}$ (b) (open gray circles). Respective Gaussian deconvolutions (dashed lines) and best fit (full black line), R = 0.9992 for $\mathbf{L^1}$ and R = 0.9986 for $\mathbf{L^2}$.

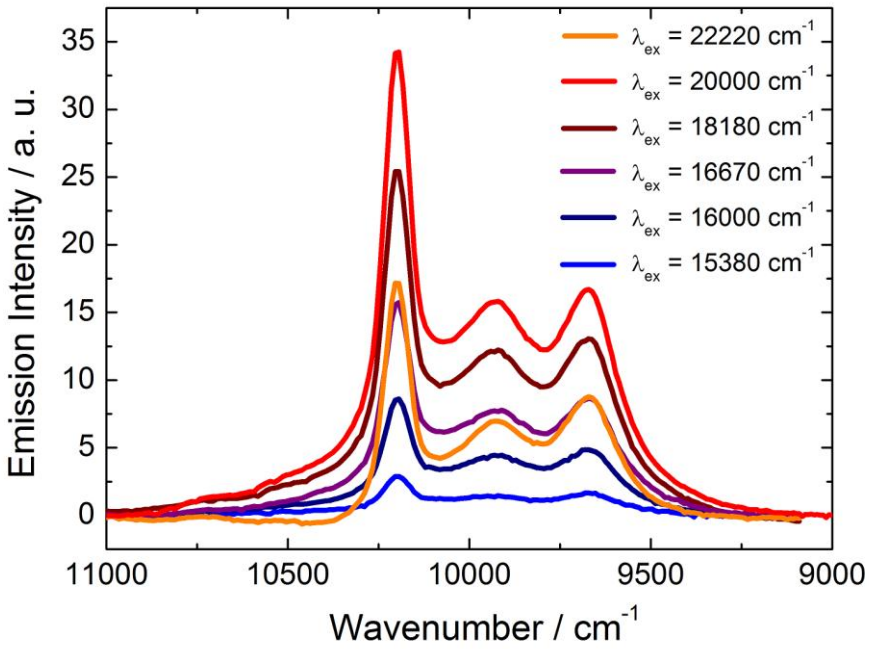

Fig. S9 Experimental solid-state emission in the near-infrared for λ_{ex} in the range of 15380-22220 cm^{-1} (450-650 nm) at room temperature.

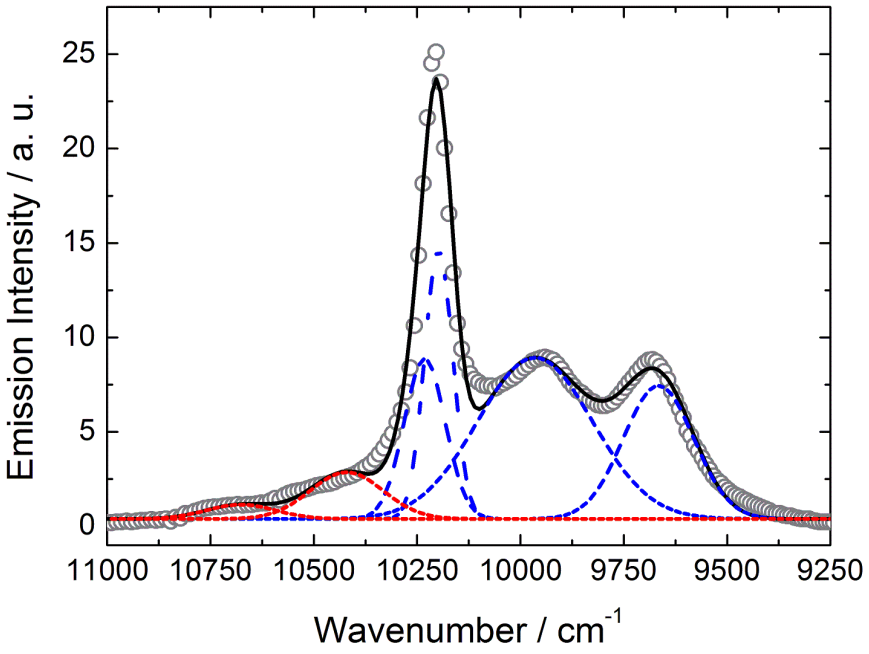

Fig. S10 Experimental solid-state emission in the near-infrared for λ_{ex} = 20000 cm^{-1} (500 nm) at room temperature (open circles), Gaussian deconvolutions (dashed lines) and best fit (full black line) R = 0.987.

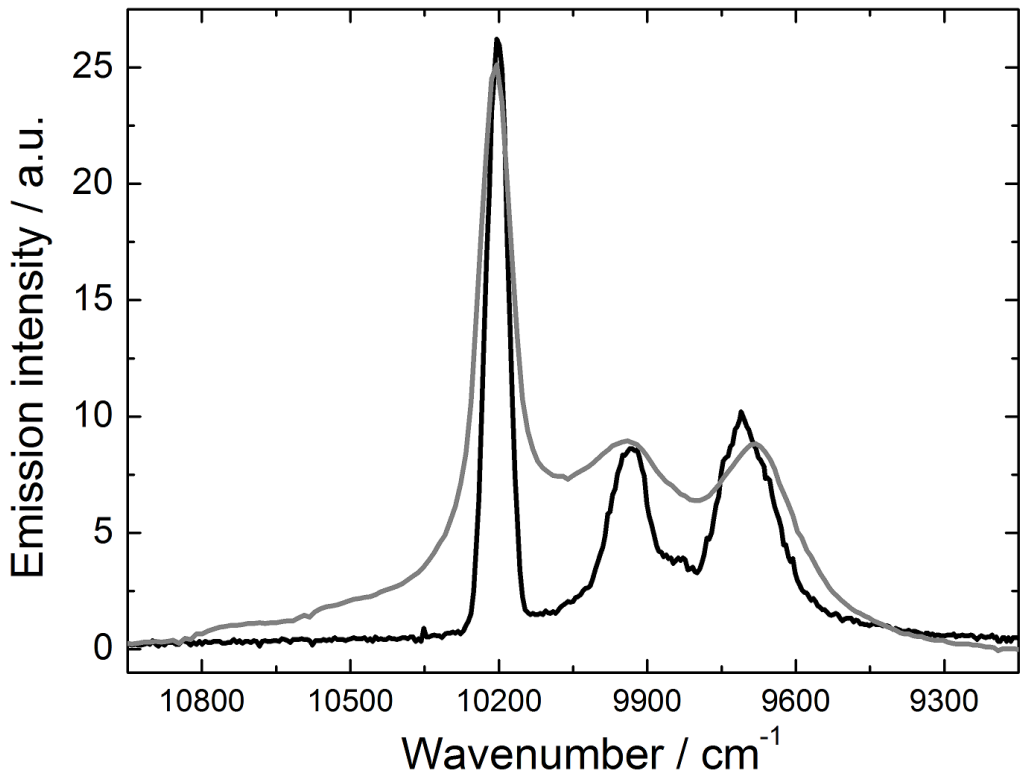

Fig. S11 Experimental solid-state emission in the near-infrared for λ_{ex} = 20000 cm^{-1} (500 nm) at room temperature (gray line) and 77 K (black line) for the dinuclear complex $[Yb(tta)_2(\mathbf{L}^1)(\mathbf{L}^2)]_2 \cdot 1.4(CH_2Cl_2)$.

Table S1. Main crystallographic parameters.

Formula	$C_{79.40}H_{56.80}Cl_{2.80}F_{12}N_4O_{16}S_{28}Yb_2$
M ($g.mol^{-1}$)	2893.91
Crystal system	Triclinic
Space group	P-1(N°2)
a(Å)	11.5275(5)
b(Å)	13.2193(5)
c(Å)	19.2725(8)
α(°)	97.1352(17)
β(°)	95.2505(16)
γ(°)	96.7382(16)
V($Å^3$)	2877.2(3)
Z	1
T(K)	150(2)
2θ(°)range	2.14-55.04
ρ($g.cm^{-3}$)	1.675
μ(Mo-Kα) (mm^{-1})	2.269
Reflns collected	33842
Independant reflns	12888
Observed reflns	10244
Parameters	724
$R_{int}/R_1/\omega R^2$	0.0389/0.0520/0.1447

Table S2. Best fitted parameters (χ_T, χ_S, τ and α) with the extended Debye model at 2000 Oe in the temperature range 1.8-5 K.

T / K	χ_T / cm^3 mol^{-1}	χ_S / cm^3 mol^{-1}	α	τ / s	R^2
1.8	1.84146	0.11992	0.26137	0.01432	0.99844
2	1.64104	0.12032	0.24991	0.01025	0.99877
2.2	1.49389	0.11327	0.23661	0.00745	0.99888
2.4	1.35105	0.10658	0.21308	0.005	0.99821
2.6	1.2535	0.10096	0.20174	0.00354	0.99824
2.8	1.13764	0.10175	0.1619	0.00238	0.99891
3	1.05567	0.10138	0.13835	0.00169	0.9993
3.2	0.98467	0.10274	0.11471	0.00122	0.99956
3.4	0.92787	0.08491	0.11204	8.53E-04	0.99949
3.6	0.87151	0.0836	0.09315	6.22E-04	0.99958
3.8	0.82794	0.07333	0.08534	4.58E-04	0.99964
4	0.78441	0.07759	0.0702	3.48E-04	0.99984
4.2	0.74784	0.07378	0.06178	2.64E-04	0.99982
4.4	0.71151	0.08411	0.04301	2.12E-04	0.99983
4.6	0.68004	0.06433	0.04643	1.56E-04	0.99988
4.8	0.65002	0.08204	0.02781	1.29E-04	0.99985
5	0.62382	0.08801	0.02761	1.04E-04	0.9999

Table S3. TD-DFT calculated excitations energies and main composition of the low-lying electronic transitions associated with an oscillator strength f>0.10, 0.08 and 0.05 for **L**^{1}, **L**^{2} and Y(III) analogue respectively. In addition it is reported the charge transfer and the pure intramolecular transitions. ID, IA, Itta^{-}, H and L represent the intramolecular BTM-TTF (Donor), COOH or CONH-2-py-*N*-oxide (Acceptor), tta- transitions, the HOMO and the LUMO respectively. Therefore ILCT stands for Intra-Ligand Charge Transfer and DACT for Donor-Acceptor Charge Transfer. The theoretical values are evaluated at the PCM(CH_2Cl_2)-PBE0/SVP level of approximation.

	E exp (cm^{-1})	E calc (cm^{-1})	Osc.	Type	Assignment	Transition
L^{1}	18300*	22774	0.05	ILCT	$\pi_{BTM-TTF}\rightarrow\pi^*_{COOH}$	H→L (98%)
	22200					
	27000	33948	0.34	ID	$\pi_{BTM-TTF}\rightarrow\pi^*_{BTM-TTF}$	H→L+3 (67%)
	33400	35665	0.11	ID	$\pi_{BTM-TTF}\rightarrow\sigma^*_{BTM-TTF}$	H→L+4 (67%)
		36204	0.11			H→L+5 (44%)
	39500	39268	0.10	ID	$\pi_{BTM-TTF}\rightarrow\pi^*_{BTM-TTF}$	H-1→L+2 (61%)
	45900	44199	0.07	ID	$\pi_{BTM-TTF}\rightarrow\pi^*_{BTM-TTF}$	H→L+6 (61%)
		45339	0.07	ILCT + ID	$\pi_{BTM-TTF}\rightarrow\pi^*_{COOH}$ + $\sigma_{BTM-TTF}\rightarrow\pi^*_{BTM-TTF}$	H-4→L (70%) H-3→L+2 (45%) H-2→L+3 (34%)
		45544	0.08			
L^{2}	18700*	21233	0.09	ILCT	$\pi_{BTM-TTF}\rightarrow\pi^*_{Py-N-oxide}$	H→L (98%)
	21500					
	27900	30474	0.24	IA	$\pi_{Py-N-oxide}\rightarrow\pi^*_{Py-N-oxide}$	H-1→L (85%)
	32300	33906	0.46	ID	$\pi_{BTM-TTF}\rightarrow\pi^*_{BTM-TTF}$	H→L+5 (54%) H-2→L (20%)
	35700	35863	0.11	ID	$\pi_{BTM-TTF}\rightarrow\pi^*_{BTM-TTF}$	H→L+6 (37%)
		36336	0.10			H→L+6/+7 (36/29%)
	38900	39150	0.12	ID	$\pi_{BTM-TTF}\rightarrow\pi^*_{BTM-TTF}$	H-2→L+3 (49%)
		39899	0.24	IA	$\pi_{Py-N-oxide}\rightarrow\pi^*_{Py-N-oxide}$	H-4→L (64%)
		41542	0.08			H-5→L (72%) H-2→L+1 (35%) H-1→L+4 (24%)
	45700	43760	0.09	ILCT	$\pi_{BTM-TTF}\rightarrow\pi^*_{Py-N-oxide}$	H-7→L (67%)
		46281	0.12			H-9→L (38%)
Y	18800	19527	0.02	LLCT	$\pi_{BTM-TTF(\mathbf{L1})}\rightarrow\pi^*_{tta}$	H→L (96%)
		20113	0.03			
	21000	20671	0.03	LLCT	$\pi_{BTM-TTF(\mathbf{L1})}\rightarrow\pi^*_{tta}$	H-3→L (30%) H-1→L+2 (55%)
		20813	0.05			
	23500	23426	0.13	ILCT	$\pi_{BTM-TTF(\mathbf{L1})}\rightarrow\pi^*_{COO-}$	H-1→L+6 (44%) H→L+9 (21%)
	27500	29502	0.12	Itta	$\pi_{tta}\rightarrow\pi^*_{tta}$	H-9→L (53%)
		30047	0.35			H-8→L+1 (36%)
		30453	0.25			H-10→L (54%)
		31111	0.29			H-11→L+1 (33%)
	30000	32093	0.44	DACT + ID	$\pi_{BTM-TTF(\mathbf{L2})}\rightarrow\pi^*_{tta}$ + $\pi_{BTM-TTF(\mathbf{L2})}\rightarrow\pi^*_{BTM-TTF(\mathbf{L2})}$	H-7→L+3 (16%) H-6→L+4 (12%)
	32500	33107	0.19	ID	$\pi_{BTM-TTF(\mathbf{L1})}\rightarrow\pi^*_{BTM-TTF(\mathbf{L2})}$	H-1→L+20 (24%) H→L+19 (17%)
		33462	0.84		$\pi_{BTM-TTF(\mathbf{L1})}\rightarrow\pi^*_{BTM-TTF(\mathbf{L1})}$	H-1→L+22 (27%)
		33993	0.21		$\pi_{BTM-TTF(\mathbf{L1})}\rightarrow\pi^*_{BTM-TTF(\mathbf{L2})}$	H-2→L+20 (29%) H-3→L+19 (27%)

* Additional band due to inter-molecular ILCT present in solid-state

1 A. I. Vooshin, N. M. Shavaleev, V. P. Kazakov, *J. Luminescence*, 2000, **91**, 49.

2 L. Russell Melby, Harris D. Hartzler, and William A. Sheppard, *J. Org. Chem*., 1974, **39**, 2457.

3 T. Devic, N. Avarvaris, P. Batail, *Eur*.-*J. Chem.*, 2004, **10**, 3697.

4 A. R. Abramovitch, B. W. Cue Jr, *J. Am. Chem. Soc.*, 1976, **17**, 1478.

5 G.M. Sheldrick, Acta Cryst. A64 (2008) 112–122. SIR97 - A. Altomare, M. C. Burla, M. Camalli, G. L. Cascarano, C. Giacovazzo, A. Guagliardi, A. G. G. Moliterni, G. Polidori, R. Spagna, *J. Appl. Cryst.*, 1999, **32**, 115.

6 M. J. Frisch, G. W. Trucks, H. B. Schlegel, G. E. Scuseria, M. A. Robb, J. R. Cheeseman, G. Scalmani, V. Barone, B. Mennucci, G. A. Petersson, H. Nakatsuji, M. Caricato, X. Li, H. P. Hratchian, A. F. Izmaylov, J. Bloino, G. Zheng, J. L. Sonnenberg, M. Hada, M. Ehara, K. Toyota, R. Fukuda, J. Hasegawa, M. Ishida, T. Nakajima, Y. Honda, O. Kitao, H. Nakai, T. Vreven, J. A. Montgomery, Jr. J. E. Peralta, F. Ogliaro, M. Bearpark, J. J. Heyd, E. Brothers, K. N. Kudin, V. N. Staroverov, R. Kobayashi, J. Normand, K. Raghavachari, A. Rendell, J. C. Burant, S. S. Iyengar, J. Tomasi, M. Cossi, N. Rega, J. M. Millam, M.; Klene, J. E. Knox, J. B. Cross, V. Bakken, C. Adamo, J. Jaramillo, R. Gomperts, R. E. Stratmann, O. Yazyev, A. J. Austin, R. Cammi, C. Pomelli, J. W. Ochterski, R. L. Martin, K. Morokuma, V. G. Zakrzewski, G. A. Voth, P. Salvador, J. J. Dannenberg, S. Dapprich, A. D. Daniels, O. Farkas, J. B. Foresman, J. V. Ortiz, J. Cioslowski D. J. Fox, Gaussian 09 Revision A.02, Gaussian Inc., Wallingford CT, 2009.

7 (a) C. Adamo, V. Barone, *J. Chem. Phys.*, 1999, **110**, 6158; (b) M. Ernzerhof, G. E. Scuseria, *J. Chem. Phys.*, 1999, **110**, 5029.

8 M. Dolg, H. Stoll, H. Preuss, *Theor. Chem. Acc.*, 1993, **85**, 441.

9 F. Weigend, R. Ahlrichs, *Phys. Chem. Chem. Phys.*, 2005, **7**, 3297.

10 J. Tomasi, B. Mennucci, R. Cammi, *Chem. Rev.*, 2005, **105**, 2999.

11 (a) M. Cossi, V. Barone, *J. Chem. Phys.*, 2001, **115**, 4708; (b) R. Improta, V. Barone, G. Scalmani, M. J. Frisch, *J. Chem. Phys.*, 2006, **125**, 054103.

12 A.-R. Allouche, *J. Comput. Chem.*, 2011, **32**, 174.

13 F. Pointillart, T. Cauchy, O. Maury, Y. Le Gal, S. Golhen, O. Cador and L. Ouahab, *Chem. Eur. J.*, 2010, **16**, 11926.